

# Resolving Weak Light of Sub-picowatt per Square Centimeter by Hybrid Perovskite Photodetectors Enabled by Noise Reduction

Yanjun Fang and Jinsong Huang\*

Organometal trihalide perovskite  $\text{CH}_3\text{NH}_3\text{PbX}_3$  (X is Cl, Br, or I) is arising as a new generation of solution processable hybrid optoelectronic material which attracts broad attention for applications in photovoltaic devices,<sup>[1–4]</sup> photodetectors,<sup>[5–7]</sup> light emitting diodes (LEDs),<sup>[8]</sup> and lasers.<sup>[9]</sup> A very rapid progress in the photovoltaic field has been witnessed by the rocketing power conversion efficiency (PCE) during the past two years with the highest certified PCE reaching 20.1% in 2014.<sup>[10]</sup> Its excellent intrinsic optoelectronic properties, including high and balanced electron and hole Hall mobilities close to those of single crystalline Si at room temperature,<sup>[11]</sup> long carrier diffusion length above 1  $\mu\text{m}$  in the polycrystalline thin films,<sup>[12]</sup> non-excitonic nature,<sup>[13]</sup> and large absorption coefficient up to  $10^5 \text{ cm}^{-1}$  in the UV–vis range,<sup>[14]</sup> which give rise to the achieved high efficiency in perovskite solar cells, in principle can also benefit its application in photodetectors. Recently, some progress has been made in applying perovskite as the active layer for photodetectors. Perovskite photodetectors with a high photoconductive gain of 300–500 were designed by either utilizing the surface charge traps induced secondary charge injection<sup>[5]</sup> or combining the perovskite light absorber with high mobility graphene.<sup>[6]</sup> Among these high gain photodetectors, the vertical structure devices have low-driving-voltage of  $<1 \text{ V}$  and a faster response speed because of the short charge transit distance. However, most of these high gain photodetectors suffer from large noise, which has limited the sensitivity of these photodetectors. For a photodetector, the most important figure-of-merit is the specific detectivity ( $D^*$ ), which characterizes how weak light it can detect. Specific detectivity is determined by the responsivity and noise of the photodetector. In another important contribution, a photodiode type perovskite photodetector with modified hole blocking layer reduces the device dark current down to  $10^{-9} \text{ A cm}^{-2}$  at bias of  $-0.1 \text{ V}$ , which resulted in a demonstrated lowest detectable light intensity of  $\approx 5 \text{ nW cm}^{-2}$ .<sup>[7]</sup>

A common practice in current studies of organic semiconductors and nanomaterials based photodetectors is to report a large specific detectivity calculated from the responsivity measured at strong light intensity and the noise by assuming it dominated by shot noise. However, this assumption might not be valid, because the high-density charge traps in the active layers

might swallow the weak light generated charges, which would dramatically reduce the device responsivity and ruin its weak irradiance detection capacity. It is shown by us that the gain (or responsivity) of a nanocomposite photodetector reduced by 10–100 times under weak light comparing to the gain under strong light due to the trap filling process.<sup>[15]</sup> Moreover, the frequency-dependent flicker noise is usually dominating the noise spectrum instead of the shot noise due to the charge trapping and detrapping process.<sup>[5]</sup> Due to these factors, the actual lowest detectable light intensity usually cannot match the high calculated specific detectivity. Considering this, it is more important to demonstrate that the photodetector can detect the light intensity as low as the noise equivalent power (NEP) to verify the high specific detectivity.

In this contribution, we reported a low noise perovskite photodetector that can directly measure the visible light intensity from around  $1 \text{ mW cm}^{-2}$  all the way down to sub  $1 \text{ pW cm}^{-2}$ , enabled by the dramatic reduction of device noise by the device interface engineering and perovskite layer morphology improvement. The double fullerene layer in the device is demonstrated to be crucial in maintaining a constant responsivity with light intensity down to  $\text{pW cm}^{-2}$  level by suppressing both shot noise and flick noise. The passivation effect of fullerene is found to be the key to realize the concurrence between the directly measured weakest light intensity and the calculated NEP for the specific detectivity.

The device structure of our perovskite photodetectors is schematically shown in **Figure 1a**. It quite resembles that of perovskite solar cells we reported previously,<sup>[3]</sup> but the electron and hole transport layers (HTLs) were intentionally modified in these photodetectors for lower dark current and noise. Briefly speaking, the poly(3,4-ethylenedioxythiophene):poly(styrenesulfonate) (PEDOT:PSS) or N4,N4'-bis(4-(6-((3-ethyloctan-3-yl)methoxy)hexyl)phenyl)-N4,N4'-diphenylbiphenyl-4,4'-diamine (OTPD) was spin-coated on to clean indium tin oxide (ITO) substrates as the HTL with a thickness of 25 or 45 nm, respectively. For the OTPD layer, an additional crosslinking process was performed to realize a compact and pin-hole free film, which also prevented it from being washed away by the solvent of the following layers. Subsequently, a 400 nm thick perovskite layer was spin-coated on to the substrates by the inter-diffusion method we developed recently.<sup>[3,4]</sup> After that, the [6,6]-phenyl-C61-butyric acid methyl ester (PCBM, 20 nm)/C<sub>60</sub> (20 or 80 nm) double fullerene layers were coated onto the perovskite films sequentially by spin-coating and thermal evaporation, respectively, to function as the electron transport layer (ETL) which also passivates the charge traps and reduce device noises as shown below. Finally, the device fabrication was finished by

Dr. Y. Fang, Prof. J. Huang  
Department of Mechanical and  
Materials Engineering  
University of Nebraska-Lincoln  
Lincoln, NE 68588, USA  
E-mail: jhuang2@unl.edu



DOI: 10.1002/adma.201500099

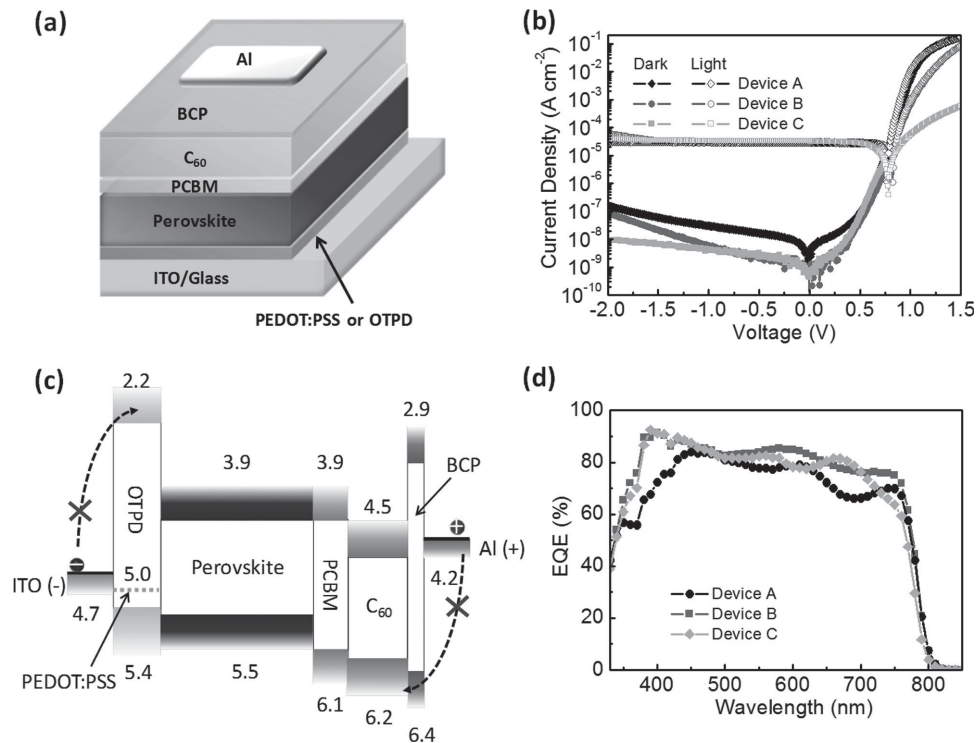


**Figure 1.** a) The schematic device structure of perovskite photodetectors. b) The dark current (solid symbols) and photocurrent density (hollow symbols, under white light  $\approx 143 \mu\text{W cm}^{-2}$ ) versus bias curves of Devices A (diamonds), B (circles), and C (squares). c) The energy diagram of the perovskite photodetectors. d) The EQE curves of Devices A (circles), B (squares), and C (diamonds) at  $-0.1 \text{ V}$  with the incident light modulation frequency of 35 Hz.

the thermal evaporation of 8 nm 2,9-dimethyl-4,7-diphenyl-1,10-phenanthroline (BCP) and 100 nm aluminum (Al) as the top electrode. In this work, three kinds of devices were fabricated with different ETLs and HTLs so that their functions in reducing device noise could be well studied: Device A with PEDOT:PSS as the HTL and PCBM/C<sub>60</sub> (20/20 nm) as the ETL, Device B with crosslinked OTPD as the HTL and PCBM/C<sub>60</sub> (20/20 nm) as the ETL, and Device C with crosslinked OTPD as the HTL and PCBM/C<sub>60</sub> (20/80 nm) as the ETL.

Figure 1b displays the dark current and photocurrent density curves (under white light of  $143 \mu\text{W cm}^{-2}$ ) of the perovskite photodetectors under the bias ranging from  $-2$  to  $1.5 \text{ V}$ . It is seen that the reverse bias dark current of Device A is already quite low, about  $1.6 \times 10^{-7} \text{ A cm}^{-2}$  under  $-2 \text{ V}$ , which is one order of magnitude lower than that of the perovskite photodetector reported previously with a similar device structure but without the C<sub>60</sub> buffer layer.<sup>[7]</sup> This clearly demonstrates that the PCBM/C<sub>60</sub> double fullerene layer can effectively reduce the dark current of perovskite photodetectors. Similar phenomenon was observed in perovskite solar cells in our previous report, which was explained by the fact that the evaporated conformal C<sub>60</sub> layer can effectively cover the rough surface of perovskite layer, so as to prevent the direct contact between the cathode and anode and reduce the leakage current.<sup>[2]</sup> The better C<sub>60</sub> coverage should also contribute to the reduction of hole injection from Al into high mobility perovskite under reverse bias, which also reduces reverse bias dark current. After replacing the HTL of PEDOT:PSS by OTPD (Device B), the dark current at  $-2 \text{ V}$  was further reduced by twofolds. More significant dark current

suppression by nearly one order of magnitude was observed under the bias lower than  $-1 \text{ V}$  compared to the Device A. Moreover, when further increasing the thickness of the C<sub>60</sub> layer to 80 nm (Device C), the dark current was suppressed to as low as  $9.1 \times 10^{-9} \text{ A cm}^{-2}$  at  $-2 \text{ V}$ , which is more than 50 times lower than the previously reported best perovskite photodetector with polymer poly[(9,9-bis(30-(*N,N*-dimethylamino)propyl)-2,7-fluorene)-alt-2,7-(9,9-dioctylfluorene)] as the ETL.<sup>[7]</sup> These results demonstrate that the buffer layer engineering at both the cathode and anode sides can effectively suppress the dark current of perovskite photodetectors, which can be understood based on the energy diagram shown in Figure 1c. Compared to the electron injection barrier of 1.1 eV between PEDOT:PSS and perovskite, it increases to 2.5 eV at the ITO/OTPD interface by replacing PEDOT:PSS with OTPD, which can effectively block the electron injection in the dark and lower the dark current. Moreover, the large hole injection barrier of 2.0 eV between Al and C<sub>60</sub> enables lower hole injection under reverse bias, and the thicker C<sub>60</sub> layer can further eliminate the leakage pathway by filling the pin-holes of the rough perovskite film, which gives rise to the even lower dark current.

Under illumination, these three types of devices show comparable photocurrent density under reverse bias despite the decreased dark current for Devices B and C, and the corresponding responsivity is around  $0.21 \text{ A W}^{-1}$  under white light, which indicates that these additional buffer layers do not impede the extraction of the photo-generated carriers. It can be explained by the large single carrier conducting capability of fullerene (for electrons) and OTPD (for holes). The

large responsivity of these devices was further confirmed by the external quantum efficiency (EQE) measurement at  $-0.1$  V bias. As shown in Figure 1d, Device A shows a high EQE of around 80% in the visible range, and Devices B and C show even higher EQE with the peak value of 93% at 390 nm. The nonflat EQE curves are caused by the absorption of ITO glass used.<sup>[4]</sup> The very large EQE above 90% at short wavelength of 390 nm even at zero bias was frequently observed in our high efficiency planar heterojunction solar cells with a same device structure with Device B. Since both Devices B and C possess the OTPD layer, the higher EQE value of these two kinds of devices, especially in the shorter wavelength range, can be explained by less charge recombination at OTPD/perovskite interface than at PEDOT:PSS/perovskite interface, due to the short penetration depth of short wavelength light. The electron–hole pairs generated by shorter wavelength light are close to the perovskite/HTL interfaces and more susceptible to charge recombination. It has been demonstrated that the perovskite based solar cells with poly[*N,N'*-bis(4-butylphenyl)-*N,N'*-bis(phenyl)benzidine] (poly-TPD) as HTL shows much better device performance than those with PEDOT:PSS.<sup>[16]</sup> Our recent study disclosed the underlying reason, which is due to the fact that perovskite films grown on wetting HTL such as PEDOT:PSS have a large density of small grains close to the PEDOT:PSS interface because the dragging force from PEDOT:PSS prevents the grain growth, which leaves a large density of charge traps at grain boundaries of the small grains.<sup>[17]</sup> On the other hand, the grains grown on nonwetting OTPD surfaces have lateral size much larger than film thickness and do not have small grains close to OTPD side, which effectively eliminates the charge recombination at OTPD/perovskite interface.<sup>[17]</sup> Therefore, the nonwetting OTPD surface can effectively change the morphology of the perovskite layer to increase the responsivity of the perovskite photodetectors. Besides, OTPD has a very low energy level of lowest unoccupied molecular orbital ( $-2.2$  eV), which can block the electrons from leaking to the anode, thus further reduce the charge recombination there.

The low dark current of our perovskite photodetectors may indicate a low noise because the shot noise ( $i_{n,s}$ ) is determined by the dark current with the following expression:<sup>[18]</sup>

$$i_{n,s} = \sqrt{2eI_d B} \quad (1)$$

where  $I_d$  is the dark current,  $e$  is the elementary charge, and  $B$  is the bandwidth. Based on dark current of the device at  $-0.1$  V, the noise is calculated to be  $5.5$  fA  $\text{Hz}^{-1/2}$ . However, as can be seen in the previously reported noise current of perovskite photodetector, the  $1/f$  noise dominates the noise current in the low frequency range.<sup>[5]</sup> Therefore, directly calculating the noise based on the dark current generally underestimates the noise of the photodetector, yielding a misleadingly higher  $D^*$  than the real value. To accurately obtain the noise current of our device with the lowest dark current (Device C), a fast Fourier transform (FFT) signal analyzer and a current preamplifier were used to record the noise current at different frequencies under  $-0.1$  V bias. It is noted the current preamplifier has a smaller noise floor at lower frequency band. Due to the very low noise of these photodetectors, only low frequency noise from 0.3 to 10 Hz can be measured, because the noise measured with wider

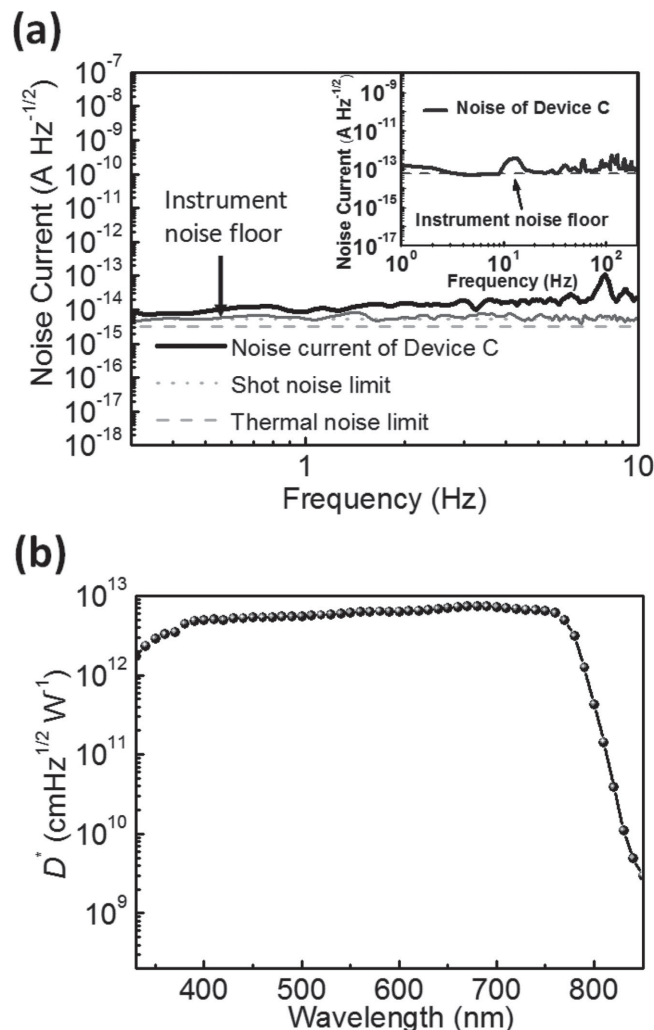


**Figure 2.** a) The measured total noise current of Device C from 0.3 to 10 Hz under  $-0.1$  V bias (black solid line), the calculated shot noise limit (gray dotted line) and thermal noise limit (gray dashed line), and the instrument noise floor (gray solid line). The inset is the measured total noise current of Device C with a wider frequency range (solid line) and the instrument noise floor with such bandwidth (dashed line) which clearly shows that the noise at higher frequency is lower than the equipment detection limit. b) The specific detectivity of Device C at different wavelength of light under  $-0.1$  V bias.

bandwidth is limited by the instrument noise floor (see inset of Figure 2a). It can be seen in Figure 2a that the noise current is independent of the frequency, and the average noise level is as low as  $16$  fA  $\text{Hz}^{-1/2}$ . The frequency independent noise indicates that the noise of the photodetector is dominated by white noise instead of  $1/f$  noise from the frequency as low as 0.3 Hz. Besides the shot noise, the thermal noise ( $i_{n,t}$ ) is also white noise and can be calculated by the following expression:<sup>[18]</sup>

$$i_{n,t} = \sqrt{\frac{4k_B T B}{R}} \quad (2)$$

where  $k_B$  is the Boltzmann constant,  $T$  is the temperature, and  $R$  is the resistance of the detector. Based on the differential

resistance at  $-0.1$  V obtained from the dark current curve, the thermal noise is calculated to be  $3.3$  fA Hz $^{-1/2}$ . Therefore, the total white noise ( $i_{n,w}$ ) calculated by the expression below is  $6.4$  fA Hz $^{-1/2}$ .<sup>[18]</sup>

$$i_{n,w} = \sqrt{i_{n,s}^2 + i_{n,t}^2} \quad (3)$$

As a result, the measured noise is very close to the calculated total noise limit by only considering the shot noise and thermal noise, and the small discrepancy may come from the noise of the measurement instruments. Since the  $1/f$  noise is generally believed to originate from carrier trapping and detrapping process,<sup>[19]</sup> the elimination of  $1/f$  noise at low frequency for our perovskite photodetector indicates the C<sub>60</sub> layer effectively passivates the surface traps of perovskite film. These results are in accordance with our thermal admittance spectroscopy measurement results where 10–1000 times less trap densities were recorded in fullerene passivated perovskite.<sup>[20]</sup> Nevertheless, a minimal C<sub>60</sub> thickness is preferred for a low noise photodetector because the charge traps in C<sub>60</sub> might also cause additional noise.

Based on the measured noise and EQE, the specific detectivity can be calculated according to the following expressions:<sup>[15]</sup>

$$D^* = \frac{\sqrt{AB}}{\text{NEP}} \quad (4)$$

$$\text{NEP} = \frac{i_n}{R_{\text{es}}} \quad (5)$$

$$R_{\text{es}} = \frac{\text{EQE}}{\frac{hc}{\lambda}} \quad (6)$$

where  $A$  is the device working area,  $i_n$  is the measured total noise,  $R_{\text{es}}$  is the responsivity,  $h$  is the Planck constant,  $c$  is the speed of light, and  $\lambda$  is the wavelength of light. As shown in Figure 2b, the specific detectivity is above  $1 \times 10^{12}$  cm Hz $^{1/2}$  W $^{-1}$  from 330 to 790 nm, with the peak value of  $7.4 \times 10^{12}$  cm Hz $^{1/2}$  W $^{-1}$  at 680 nm. This value is comparable to the commercial Si photodiode at the same wavelength,<sup>[15]</sup> demonstrating its potential application in weak visible light sensing.

Based on the high  $D^*$  demonstrated above, the NEP of our perovskite photodetector is calculated to be  $4.3 \times 10^{-14}$  W Hz $^{-1/2}$  at the wavelength of 560 nm, which means that the photodetector should be able to detect the green light intensity as low as  $0.6$  pW cm $^{-2}$  considering the device working area of  $7.25$  mm $^2$ . However, this is valid only when the photodetector keeps a constant responsivity even under very weak illumination close to NEP. So it is essential to verify whether the photodetector can detect light intensity as low as NEP, which is, however, missing in many recent publications. Here we tested whether the calculated NEP actually agrees with our device's detection limit by developing a new method to directly measure the NEP of the photodetectors. We recorded the total current of the photodetector (Device C) at  $-0.1$  V under various light intensities with the FFT signal analyzer in the same way we measured the noise. During the measurement, the incident light from a

green LED (emission peak at 560 nm) was modulated to be 6 Hz by a function generator and the light intensity was severely attenuated by neutral density filters. It is expected that a peak at the frequency of 6 Hz will appear in the current spectrum when turning on the LED, and its peak intensity should be proportional to the photocurrent of the device. According to the definition of NEP, it represents the lowest light intensity under which the photocurrent can no longer be differentiated from the noise current. As a result, when the light intensity is decreased to a value that the peak at 6 Hz is merged into the background noise current, this light intensity can be considered as the NEP of the device. As can be seen in Figure 3a, there is a peak at the frequency of 6 Hz in the current spectrum and its intensity gradually reduces with decreasing the incident light intensity. The irradiance-dependent signal intensity at 6 Hz is plotted in Figure 3b, which shows that the signal peak intensity decreases linearly with the light intensity, and the lowest detectable light intensity is  $\approx 0.64$  pW cm $^{-2}$ , which is almost the same as the calculated NEP. To the best of our knowledge, this is the first time that the directly measured NEP can agree with the calculated one for perovskite photodetectors, and the measured NEP value is more than 6 orders of magnitude lower than that of the previously reported perovskite-graphene hybrid photodetectors,<sup>[6]</sup> almost 3–4 orders of magnitude lower than those of other perovskite photodiodes reported<sup>[7,21]</sup> and also 1 order of magnitude lower than that of the high-gain low-driving-voltage perovskite photodetector.<sup>[5]</sup> It is noted perovskite photodetectors with a similar structure were reported,<sup>[21]</sup> while our device showed much higher sensitivity because of our excellent reduction of noise by trap passivation by fullerene as well as excellent crystallinity of perovskite grains.

The linear dynamic range (LDR), which represents the light intensity range between which the responsivity of the photodetector keeps constant, was measured by recording the photocurrent change of the Device C under various green light intensities with the modulation frequency of 35 Hz by a lock-in amplifier. Figure 3c shows that the photocurrent increases linearly with increasing the light intensity from around  $1$  pW cm $^{-2}$  to above  $1$  mW cm $^{-2}$ , yielding a large LDR of 94 dB calculated by:<sup>[18]</sup>

$$\text{LDR} = 10 \log \frac{P_{\text{sat}}}{\text{NEP}} \quad (7)$$

where  $P_{\text{sat}}$  is the saturation signal power, i.e., the light intensity under which the photocurrent began to deviate from linearity. This is the largest LDR ever reported for a perovskite photodetector. With further increasing the light intensity to above  $3$  mW cm $^{-2}$ , the responsivity of the photodetector began to drop, which is probably due to the thick low mobility C<sub>60</sub> layer that hinders the extraction of the high density photogenerated electrons under strong irradiance. Besides, the photocurrent hysteresis is a critical issue in accurately determining the perovskite solar cell efficiency,<sup>[22]</sup> which may also hamper the reliable operation of perovskite photodetectors. To find out whether our photodetector can output the reproducible photocurrent under repeated measurement in weak irradiance, we measured the photocurrent of the device under first increasing then decreasing, and

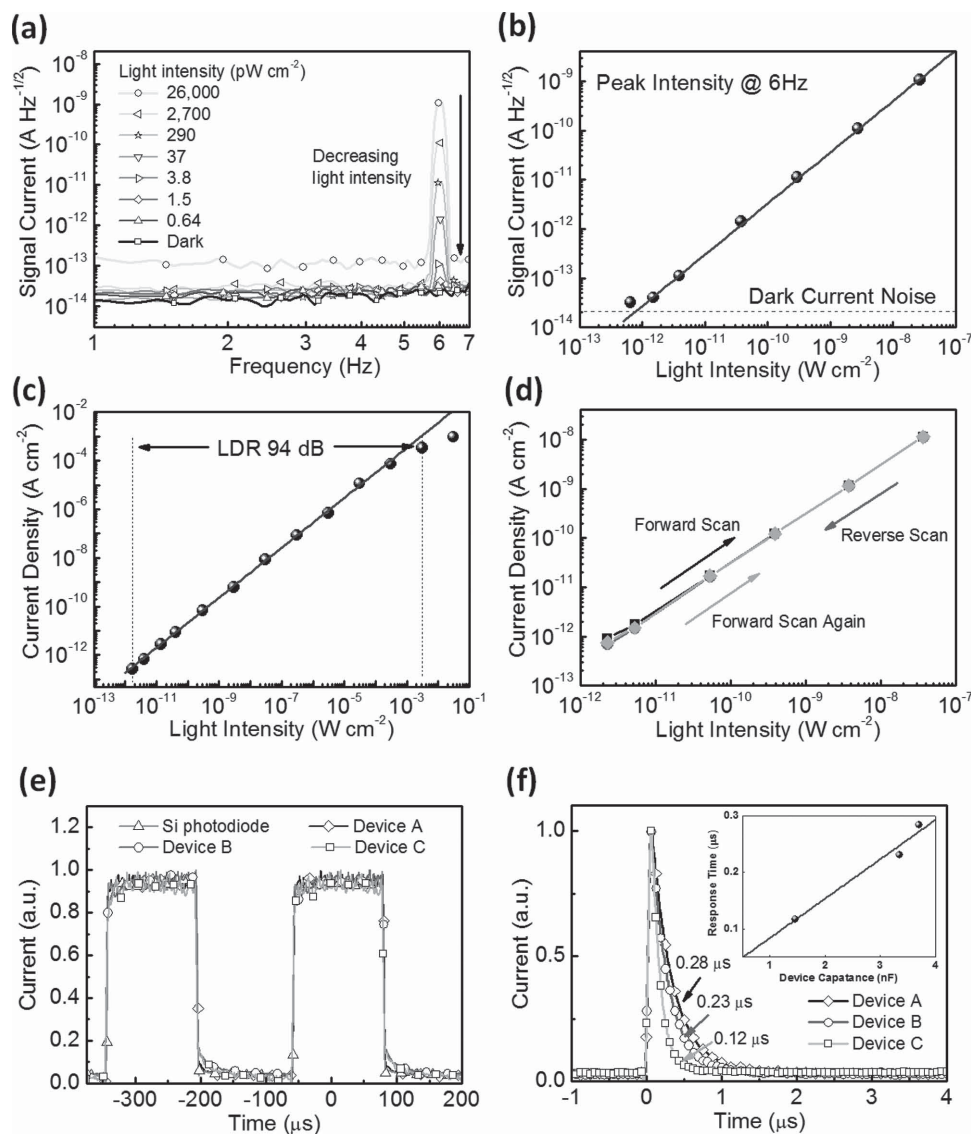


**Figure 3.** a) The current spectra of Device C at  $-0.1$  V under 560 nm light illumination modulated at 6 Hz with various light intensities for direct NEP measurement. b) The peak signal intensity at 6 Hz obtained from (a) as a function of light intensities. The solid line is a linear fitting to the data and the dashed line is the dark current noise level. c) The dynamic range measurement of Device C at  $-0.1$  V with green light illumination of various light intensities. The solid line is a linear fitting to the data. d) The repeated photocurrent scans of Device C with both increasing and decreasing light intensities under weak illumination. e) The transient photocurrent curves of Devices A (diamonds), B (circles), C (squares), and Si photodiode (triangles) measured under the illumination of a chopper modulated 532 nm laser at 3500 Hz. f) The transient photocurrent curves of Devices A (diamonds), B (circles), and C (squares) measured with a 337 nm 4 ns-pulse laser as the light source. The inset is the device response time as a function of capacitance of the devices and the solid line is a linear fitting to the data.

again increasing light intensity in the weak light region (light intensity  $< 30$  nW  $\text{cm}^{-2}$ ), and the device shows excellent output reproducibility (Figure 3d). This is in good accordance with our previous photocurrent measurement of perovskite solar cells that also shows no hysteresis, which is owing to the trap passivation effect of the double fullerene layer.<sup>[20]</sup>

Finally, the response speed of the perovskite photodetectors was measured by transient photocurrent method. The devices were under the chopper modulated 532 nm laser illumination at the frequency of 3500 Hz, and the transient photocurrent signal was recorded by an oscilloscope. The measurement was also performed on a commercial Si photodiode to determine

the switching speed of the chopper. It is seen in Figure 3e that the three kinds of perovskite photodetectors (Devices A, B, and C) show almost the same response speed as the Si photodiode, with the photocurrent rise and fall time less than 5  $\mu\text{s}$ . This value is in well accordance with the calculated switching time of the chopper, which indicates that the response speed measurement of the photodetectors is limited by the chopper speed. To remove the modulation speed limitation of light source and accurately determine the response speed of the devices, a 337 nm pulse laser with the pulse width less than 4 ns was used to replace the continuous laser as the light source, and corresponding device response curves are shown in Figure 3f.

By fitting the photocurrent decay curves with the single exponential decay function, the response time of the Devices A, B, and C are derived to be 280, 230, and 120 ns, respectively. It is surprising that Device C with the thickest  $C_{60}$  layer shows the fastest response speed, indicating that the response time may be limited by the resistor–capacitor (RC) time constant of the circuit instead of the low carrier mobility buffer layers. To verify this speculation, we first calculated the electron transit time across the device based on the following expression:

$$t_{tr} = \frac{d^2}{\mu V} \quad (8)$$

where  $t_{tr}$  is the charge transit time,  $\mu$  is the carrier drift mobility, and  $V$  is the voltage. Considering the orders of magnitude higher drift mobility of perovskite than  $C_{60}$ ,<sup>[23]</sup> only the drift time in  $C_{60}$  layer is considered here. Using a moderate electron mobility of  $1 \times 10^{-3} - 1 \times 10^{-2} \text{ cm}^2 \text{ V}^{-1} \text{ s}^{-1}$  for  $C_{60}$ , and the built-in potential of about 1 V, the  $t_{tr}$  is calculated to be 6.4–64 ns, lower than the measured response time. In fact, even lower response time around 7 ns was reported for a carbon nanotube based photodetector under 0 V bias with a thicker  $C_{60}$  buffer layer of 100 nm.<sup>[24]</sup> Hence our device's response speed should not be limited by the thick  $C_{60}$  layer. Then, the capacitance of the Devices A, B, and C was measured by an inductance–capacitance–resistance (LCR) meter at 100 kHz, and correlation between the response time and the device capacitance is shown in the inset of Figure 3f. It is seen that the response time increases linearly with the device capacitance. Considering the capacitance of Device C of 1.5 nF, and the input impedance of the oscilloscope of 50  $\Omega$ , the RC time constant of the circuit for Device C is 75 ns, close to the measured response time of 120 ns. The discrepancy may arise from the other series resistance in the circuit. Based on the response time of 120 ns for Device C, its 3-dB cut-off frequency ( $f_{3dB}$ ) can be calculated by:<sup>[18]</sup>

$$f_{3dB} = \frac{0.35}{t_R} \quad (9)$$

where  $t_R$  is the response time of the device. The 3-dB cut-off frequency is calculated to be 2.9 MHz for Device C, which is the same as the previously reported perovskite photodetector with a much smaller working area.<sup>[7]</sup> In the future, the response speed may be further improved by reducing the working area of the device to decrease the device capacitance.

The device stability, which is a major concern in the development of perovskite based solar cells, is also very important for the practical application of perovskite-based photodetectors. Here we monitored the change of the photocurrent and dark current of the non-encapsulated devices after storage in  $N_2$ -filled glove-box for about 45 days, and the typical current density–voltage curves are shown in Figure S1 in the Supporting Information. It is clearly seen that there is almost no discernible degradation in the photocurrent and dark current of the device after long time storage, which indicates its excellent temporal stability. Besides, most of the device performance measurements, like noise, NEP, LDR, and temporal response, were conducted in air without encapsulation, indicating the good air

stability of the device. It is expected that the longtime air stability of the device can be further improved through encapsulation, which has already been demonstrated in ref. [25].

In summary, a highly sensitive perovskite photodetector has been reported here with low noise (16 fA  $\text{Hz}^{-1/2}$  at  $-0.1$  V) close to the shot and thermal noise limits, high average EQE approaching 90%, large LDR of 94 dB and short response time of 120 ns. The interfacial ETL and HTL engineering of the device, especially the trap passivation effect of the fullerene layer, enables its direct measurement of light irradiance down to sub 1 pW  $\text{cm}^{-2}$ , which matches well with the calculated NEP. The excellent weak light sensing capability of the perovskite photodetector makes it potential in replacing commercial Si photodiodes in the applications like defense, communication, and imaging.

## Supporting Information

Supporting Information is available from the Wiley Online Library or from the author.

## Acknowledgements

This work was supported by the Defense Threat Reduction Agency (Award No. HDTRA1-10-1-0098) and the Office of Naval Research (ONR, Award No. N000141210556).

Received: January 8, 2015

Revised: February 16, 2015

Published online: March 18, 2015

- [1] a) J. Burschka, N. Pellet, S.-J. Moon, R. Humphry-Baker, P. Gao, M. K. Nazeeruddin, M. Grätzel, *Nature* **2013**, 499, 316; b) M. Liu, M. B. Johnston, H. J. Snaith, *Nature* **2013**, 501, 395; c) C. Bi, Y. Yuan, Y. Fang, J. Huang, *Adv. Energy Mater.* **2014**, DOI: 10.1002/aenm.201401616; d) H. Zhou, Q. Chen, G. Li, S. Luo, T.-b. Song, H.-S. Duan, Z. Hong, J. You, Y. Liu, Y. Yang, *Science* **2014**, 345, 542; e) Z. Xiao, Y. Yuan, Y. Shao, Q. Wang, Q. Dong, C. Bi, P. Sharma, A. Gruverman, J. Huang, *Nat. Mater.* **2015**, 14, 193.
- [2] Q. Wang, Y. Shao, Q. Dong, Z. Xiao, Y. Yuan, J. Huang, *Energy Environ. Sci.* **2014**, 7, 2359.
- [3] Z. Xiao, C. Bi, Y. Shao, Q. Dong, Q. Wang, Y. Yuan, C. Wang, Y. Gao, J. Huang, *Energy Environ. Sci.* **2014**, 7, 2619.
- [4] Z. Xiao, Q. Dong, C. Bi, Y. Shao, Y. Yuan, J. Huang, *Adv. Mater.* **2014**, 26, 6503.
- [5] R. Dong, Y. Fang, J. Chae, J. Dai, Z. Xiao, Q. Dong, Y. Yuan, A. Centrone, X. C. Zeng, J. Huang, *Adv. Mater.* **2015**, 27, 1912.
- [6] Y. Lee, J. Kwon, E. Hwang, C.-H. Ra, W. J. Yoo, J.-H. Ahn, J. H. Park, J. H. Cho, *Adv. Mater.* **2015**, 27, 41.
- [7] L. Dou, Y. Yang, J. You, Z. Hong, W.-H. Chang, G. Li, *Nat. Commun.* **2014**, 5, 5404.
- [8] Z.-K. Tan, R. S. Mghaddam, M. L. Lai, P. Docampo, R. Higler, F. Deschler, M. Price, A. Sadhanala, L. M. Pazos, D. Credgington, F. Hanusch, T. Bein, H. J. Snaith, R. H. Friend, *Nat. Nanotechnol.* **2014**, 9, 687.
- [9] G. Xing, N. Mathews, S. S. Lim, N. Yantara, X. Liu, D. Sabba, M. Grätzel, S. Mhaisalkar, T. C. Sum, *Nat. Mater.* **2014**, 13, 476.
- [10] Best Research-Cell Efficiency, [http://www.nrel.gov/ncpv/images/efficiency\\_chart.jpg](http://www.nrel.gov/ncpv/images/efficiency_chart.jpg), accessed: December 2014.

- [11] C. C. Stoumpos, C. D. Malliakas, M. G. Kanatzidis, *Inorg. Chem.* **2013**, *52*, 9019.
- [12] S. D. Stranks, G. E. Eperon, G. Grancini, C. Menelaou, M. J. P. Alcocer, T. Leijtens, L. M. Herz, A. Petrozza, H. J. Snaith, *Science* **2013**, *342*, 341.
- [13] V. D'Innocenzo, G. Grancini, M. J. P. Alcocer, A. R. S. Kandada, S. D. Stranks, M. M. Lee, G. Lanzani, H. J. Snaith, A. Petrozza, *Nat. Commun.* **2014**, *5*, 3586.
- [14] M. A. Green, A. Ho-Baillie, H. J. Snaith, *Nat. Photonics* **2014**, *8*, 506.
- [15] F. Guo, B. Yang, Y. Yuan, Z. Xiao, Q. Dong, Y. Bi, J. Huang, *Nat. Nanotechnol.* **2012**, *7*, 798.
- [16] D. Zhao, M. Sexton, H.-Y. Park, G. Baure, J. C. Nino, F. So, *Adv. Energy Mater.* **2014**, DOI: 10.1002/aenm.201401855.
- [17] C. Bi, Q. Wang, Y. Shao, Y. Yuan, J. Huang, unpublished.
- [18] *Photonic Devices*, (Ed: J.-M. Liu), Cambridge University Press, Cambridge, UK **2005**.
- [19] C. T. Lin, Y. K. Su, S. J. Chang, H. T. Huang, S. M. Chang, T. P. Sun, *IEEE Photonics Technol. Lett.* **1997**, *9*, 232.
- [20] Y. Shao, Z. Xiao, C. Bi, Y. Yuan, J. Huang, *Nat. Commun.* **2014**, *5*, 5784.
- [21] Q. Lin, A. Armin, D. M. Lyons, P. L. Burn, P. Meredith, *Adv. Mater.* **2015**, *12*, 2060.
- [22] H. J. Snaith, A. Abate, J. M. Ball, G. E. Eperon, T. Leijtens, N. K. Noel, S. D. Stranks, J. T.-W. Wang, K. Wojciechowski, W. Zhang, *J. Phys. Chem. Lett.* **2014**, *5*, 1511.
- [23] C. Wehrenfennig, G. E. Eperon, M. B. Johnston, H. J. Snaith, L. M. Herz, *Adv. Mater.* **2014**, *26*, 1584.
- [24] M. S. Arnold, J. D. Zimmerman, C. K. Renshaw, X. Xu, R. R. Lunt, C. M. Austin, S. R. Forrest, *Nano Lett.* **2009**, *9*, 3354.
- [25] Y. Guo, C. Liu, H. Tanaka, E. Nakamura, *J. Phys. Chem. Lett.* **2015**, *6*, 535.